Corrections

BIOPHYSICS AND COMPUTATIONAL BIOLOGY

Correction for "Structural defects and the diagnosis of amyloidogenic propensity," by Ariel Fernández, József Kardos, L. Ridgway Scott, Yuji Goto, and R. Stephen Berry, which appeared in issue 11, May 27, 2003, of *Proc Natl Acad Sci USA* (100:6446–6451; first published May 12, 2003; 10.1073/pnas.0731893100).

The undersigned authors note the following: "We wish to bring to your attention an issue regarding our PNAS publication referenced above. Although we cite our earlier PNAS publication (see ref. 23 therein), portions of the text and figures are similar to ref. 23 and were not properly attributed. Ref. 23 reports an experimental result, while the paper indicated above reports theoretical work. Nevertheless, in the examples below we should have provided a citation to ref. 23 as the source of the information.

"Fig. 2 was adapted from Fig. 1 in ref. 23. Fig. 5 was adapted from Fig. 2 in ref. 23.

"The following text in the section titled 'Structure Wrapping and Molecular Disease' on page 6447 of our text is similar to the text in the fifth paragraph of the "Results and Discussion" section on page 2392 in ref. 23:

> Figs. 2 and 3 display the UWHBs for Hb β-subunit (pdb.1bz0, chain B) and human cellular prion protein (pdb.1qm0) (12–14). Within the natural interactive context of the Hb subunit, the UWHBs signal crucial binding regions (24): UWHBs (*90*, *94*), (*90*, *95*) are associated with the β-FG corner involved in the quaternary $\alpha1\beta2$ interface; UWHB (*5*, *9*) is adjacent to Glu-6 which in sickle cell anemia mutates to Val-6 and is located at the Val-6-(Phe-85, Leu-88) interface in the deoxyHbS fiber.

"The following text in the section titled 'Toward a Structural Diagnosis' on page 6449 of our text is similar to the text beginning in the last paragraph on page 2392 in ref. 23:

> The distribution of proteins according to their average extent of hydrogen bond wrapping and their spatial concentration of structural defects is shown in Fig. 5 (see also ref. 23). The sample of 2,811 PDB proteins is large enough to define a reliable abundance distribution with an inflection point at $\rho = 6.20$. The integration of the distribution over a ρ-interval gives the fraction of proteins whose ρ lies within that range. Of the 2,811 proteins examined, 2,572 have $\rho > 6.20$, and none of them is known to yield amyloid aggregation under physiological conditions entailing partial retention of structure. Strikingly, relatively few disease-related amyloidogenic proteins are known in the sparsely populated, underwrapped $3.5 < \rho < 6.20$ range, with the cellular prion proteins located at the extreme of the spectrum ($3.53 < \rho < 3.72$)....
>
> The range of H-bond wrapping $3.5 < \rho < 4.6$ of 20 sampled PDB membrane proteins has been included in Fig. 5 for comparison. As expected, such proteins do not have the stringent H-bond packing requirements of soluble proteins for their H bonds at the lipid interface. Thus, this comparison becomes suggestive in terms of elucidating the driving factor for aggregation in soluble proteins: Although the UWHB constitutes a structural defect in a soluble protein because of its vulnerability to water attack, it is not a structural defect in a membrane protein. The exposure of the polar amide and carbonyl of the unbound state to a nonpolar phase is thermodynamically unfavorable (22). The virtually identical ρ value for human prion and outer-membrane protein A (Fig. 5) is revealing in this regard.
>
> Furthermore, all known amyloidogenic proteins that occur naturally in complexed form have sufficient H-bond wrapping within their respective complexes (ρ value near 6.2). Their amyloidogenic propensity appears only under conditions in which the protein is dissociated from the complex (compare Fig. 5). This finding is corroborated by the following computation. If an intramolecular hydrogen bond is underwrapped within the isolated protein molecule but located at an interface upon complexation, then to determine its extent of wrapping within the complex, we take into account the additional residues in the binding partner that lie within the desolvation domain of the intramolecular H bond. Thus, the uncomplexed or monomeric β_2-microglobulin (pdb. 1i4f) (21) has $\rho = 5.2$, putting it in the purported amyloidogenic region. However, upon complexation within the MHC-I, its ρ increases to 6.22.

"The original work on the diagnosis of amyloidogenic propensity was carried out in the summer of 2002 at Osaka University. We apologize for not alerting readers of the similarities between these two texts."

Ariel Fernandez
R. Stephen Berry

www.pnas.org/cgi/doi/10.1073/pnas.1112740108

BIOPHYSICS AND COMPUTATIONAL BIOLOGY

Correction for "Protein–protein interface-binding peptides inhibit the cancer therapy target human thymidylate synthase," by Daniela Cardinale, Giambattista Guaitoli, Donatella Tondi, Rosaria Luciani, Stefan Henrich, Outi M. H. Salo-Ahen, Stefania Ferrari, Gaetano Marverti, Davide Guerrieri, Alessio Ligabue, Chiara Frassineti, Cecilia Pozzi, Stefano Mangani, Dimitrios Fessas, Remo Guerrini, Glauco Ponterini, Rebecca C. Wade, and M. Paola Costi, which appeared in issue 34, August 23, 2011, of *Proc Natl Acad Sci USA* (108:E542–E549; first published July 27, 2011; 10.1073/pnas.1104829108).

The authors note that the acknowledgment "LIGHTS project: LSH-2005-2.2.0-8" should instead appear as "LIGHTS project: LSHC-CT-2006-037852."

www.pnas.org/cgi/doi/10.1073/pnas.1113637108

ECOLOGY

Correction for "Global distribution and conservation of marine mammals," by Sandra Pompa, Paul R. Ehrlich, and Gerardo Ceballos, which appeared in issue 33, August 16, 2011, of *Proc Natl Acad Sci USA* (108:13600–13605; first published August 1, 2011; 10.1073/pnas.1101525108).

The authors note the following statement should be added to the Acknowledgments: "We are thankful for the academic support given to this PhD research by the Posgrado en Ciencias Biológicas (Universidad Nacional Autónoma de México)."

www.pnas.org/cgi/doi/10.1073/pnas.1112899108

GENETICS

Correction for "Targets of the transcriptional repressor oncoprotein Gfi-1," by Zhijun Duan and Marshall Horwitz, which appeared in issue 10, May 13, 2003, of *Proc Natl Acad Sci USA* (100:5932–5937; first published April 29, 2003; 10.1073/pnas.1031694100).

The authors note that, during the course of preparation of Figs. 1 and 2, some of the individual panels depicting EMSAs were inadvertently duplicated. The problem was recently discovered and is now corrected with new scans from films recording the original electropherograms. These errors do not affect the conclusions of the article. The corrected figures and their respective legends appear below.

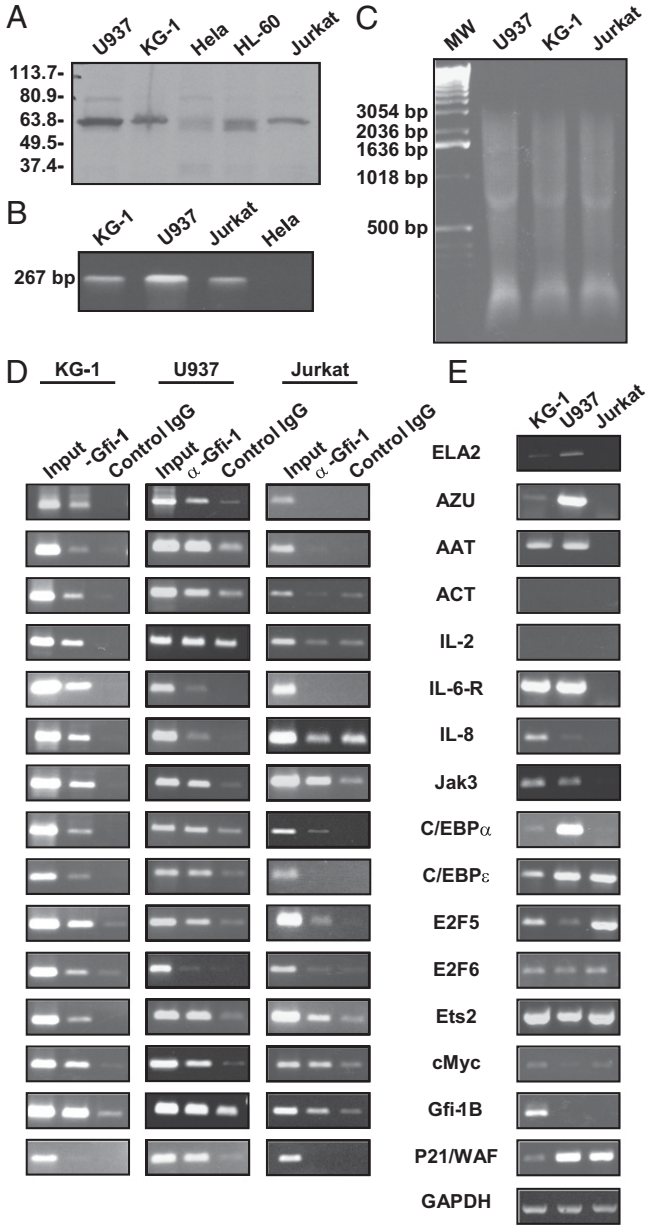

Fig. 1. Gfi-1 target genes. (*A*) Expression of Gfi-1 protein, Western blot. (*B*) Expression of Gfi-1 transcript, RT-PCR. (*C*) Sonicated chromatin used as input for ChIP assay, ethidium bromide-stained agarose gel. (*D*) ChIP assays, representative results. In the revised figure, panels depicting Gfi-1B (U937), IL-8 (Jurkat), IL-2 (U937), E2F5 (Jurkat), and C/EBPe (Jurkat), which had been aberrantly duplicated, have been replaced with scans from photographs of the original ethidium bromide-stained agarose gels. (*E*) Semiquantitative RT-PCR of Gfi-1 target genes with GAPDH control. In the revised figure, panels showing ELA2 and JAK3, which had been aberrantly duplicated, have been replaced with scans from photographs of the original ethidium bromide-stained agarose gels.

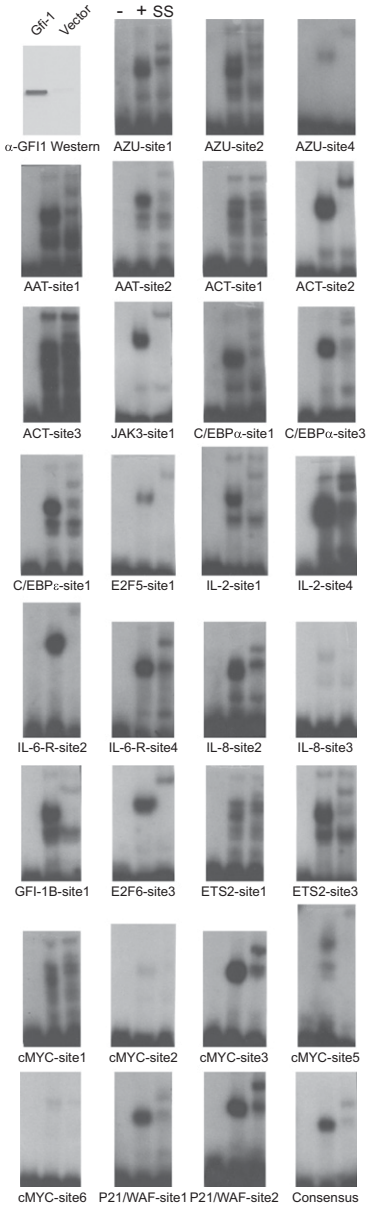

Fig. 2. Characterization of Gfi-1 binding sites in target genes by EMSA. (*Upper Left*) α-Gfi-1 Western blot of in vitro synthesized Gfi-1 compared with TnT transcription/translation system programmed with vector-only control. EMSA was performed with oligonucleotides listed in Table S3. The first lane (–) of the remaining 31 panels shows DNA probe alone; the second lane (+) shows addition of TnT-synthesized Gfi-1; and the third lane is supershift with α-Gfi-1 antibody. Negative results for 30 other tested potential binding sites are not shown. In the original image, multiple panels were aberrantly duplicated; to avoid confusion, a replacement figure has been constructed using all new scans of original X-ray film recording the autoradiograms.

www.pnas.org/cgi/doi/10.1073/pnas.1112888108

Protein–protein interface-binding peptides inhibit the cancer therapy target human thymidylate synthase

Daniela Cardinale[a], Giambattista Guaitoli[a], Donatella Tondi[a], Rosaria Luciani[a], Stefan Henrich[b], Outi M. H. Salo-Ahen[b], Stefania Ferrari[a], Gaetano Marverti[c], Davide Guerrieri[c], Alessio Ligabue[c], Chiara Frassineti[c], Cecilia Pozzi[d], Stefano Mangani[d], Dimitrios Fessas[e], Remo Guerrini[f], Glauco Ponterini[g,1], Rebecca C. Wade[b,1], and M. Paola Costi[a,1]

[a]Department of Pharmaceutical Sciences, via Campi 183, University of Modena and Reggio Emilia, 41126 Modena, Italy; [b]Molecular and Cellular Modeling Group, Heidelberg Institute for Theoretical Studies, Schloss-Wolfsbrunnenweg 35, 69118 Heidelberg, Germany; [c]Department of Biomedical Sciences, via Campi 287, University of Modena and Reggio Emilia, 41126 Modena, Italy; [d]Department of Chemistry, University of Siena, via Aldo Moro 2, 53100 Siena, Italy; [e]Department of Food Science, Technology and Microbiology, University of Milan, via Celoria 2, 20133 Milan, Italy; [f]Department of Pharmaceutical Sciences, University of Ferrara, via Fossato di Mortara 17-19, 44100 Ferrara, Italy; and [g]Department of Chemistry, via Campi 183, University of Modena and Reggio Emilia, 41126 Modena, Italy

Edited* by Robert M. Stroud, University of California, San Francisco, CA, and approved June 30, 2011 (received for review March 28, 2011)

Human thymidylate synthase is a homodimeric enzyme that plays a key role in DNA synthesis and is a target for several clinically important anticancer drugs that bind to its active site. We have designed peptides to specifically target its dimer interface. Here we show through X-ray diffraction, spectroscopic, kinetic, and calorimetric evidence that the peptides do indeed bind at the interface of the dimeric protein and stabilize its di-inactive form. The "LR" peptide binds at a previously unknown binding site and shows a previously undescribed mechanism for the allosteric inhibition of a homodimeric enzyme. It inhibits the intracellular enzyme in ovarian cancer cells and reduces cellular growth at low micromolar concentrations in both cisplatin-sensitive and -resistant cells without causing protein overexpression. This peptide demonstrates the potential of allosteric inhibition of hTS for overcoming platinum drug resistance in ovarian cancer.

allosteric mechanism | peptide design | protein–protein interface inhibitor

Enzymes whose catalytic activity depends on multimeric assembly are targets for inhibitors that perturb the interactions between the protein subunits. The high diversity of protein interfaces implies opportunities for the identification of specific inhibitors (1–5). The design of peptides and peptidomimetics that mimic portions of these interfaces has been shown to be a useful approach for the discovery of inhibitors that bind at protein–protein interfaces (5–11). However, the inhibitory mechanism of such ligands is often unclear, and the binding geometry does not necessarily correspond to that mimicked.

Human thymidylate synthase (hTS) is an enzyme in the folate pathway that catalyses the reductive methylation of 2′-deoxyuridine-5′-monophosphate (dUMP) to form 2′-deoxythymidine-5′-monophosphate (dTMP). This methylation reaction is assisted by the cofactor N^5, N^{10}-methylenetetrahydrofolate (mTHF) (12). hTS is an obligate homodimer whose monomers can adopt active (A) and inactive (I) forms (13–15). The hTS dimer has two active sites, each formed by residues from both monomers. Therefore the dimeric assembly is necessary for the catalytic activity. The hTS dimer-to-monomer dissociation constant (K_d) was recently reported to be 200 nM (16). The active and inactive forms differ in the conformation of the loop from residue 181 to residue 197, which contains the catalytic cysteine, residue 195. This residue points into the active site in the active form and toward the dimer interface in the inactive form (13–15). Active-site inhibitors of hTS are widely used in chemotherapy; the best known are raltitrexed, pemetrexed, and 5-fluorouracil (5FU), a prodrug of the active 5-fluoro-2′-deoxyuridine-5′-monophosphate (FdUMP) (17). In addition to its catalytic role, hTS has been shown to regulate protein synthesis by interacting with its own mRNA as well as the mRNAs of several other proteins involved in the cell cycle (18–21). The regulatory function of hTS as an RNA binding protein has been shown to be maximal when the protein is ligand-free (22). This observation, together with the observation that cancer cells resistant to anti-hTS drugs showed increased levels of hTS, led to the suggestion that the overexpression of hTS is correlated with the loss of RNA regulatory capacity when the protein is bound to its inhibitors (19, 21, 23, 24). In the case of 5FU, a covalent hTS inhibitor, high hTS protein levels were attributed to both mRNA regulation and a decrease in enzyme degradation efficiency caused by inhibitor binding (15, 25). These studies were performed on colon cancer cells, but clinical and biochemical observations suggest similar behavior occurs in other cancer types, such as ovarian cancer. The latter is a severe pathology with a high mortality rate, which is due to frequent late diagnosis and the rapid development of drug resistance (26, 27). Access to therapy has been limited by the cross-resistance of platinum drugs with classical drugs that target the folate pathway (28–30). In recent years, clinical trials have demonstrated the effectiveness of the combination of carboplatin or cisplatin (cDDP) and pemetrexed, a multitargeted antifolate drug, for the treatment of platinum-sensitive and -resistant ovarian cancers (31, 32). Although overexpression of hTS has been observed in platinum-sensitive cells, this effect is even more pronounced in platinum-resistant ones. Therefore, it is important to identify hTS inhibitors that act through new mechanisms that do not alter RNA regulation or increase protein levels. With this aim, some diphosphonic acids have been proposed as allosteric inhibitors of hTS (33). The most active one is 1,3-propanediphosphonic acid (PDPA) which binds at the position where the phosphate group of dUMP binds. However, the mechanism of inhibition of these compounds has not yet been biochemically and mechanistically demonstrated; furthermore, PDPA has no cellular activity, and thus its potential as a drug is limited.

In this paper, we describe the discovery of several peptides, with sequences from the hTS dimer interface, that inhibit hTS by a mechanism that involves selective binding to a previously undescribed allosteric binding site at the dimer interface of the di-inactive form of the enzyme. The mechanism is demonstrated by X-ray diffraction, CD and fluorescence spectroscopies, kinetic

Author contributions: D.T., G.P., R.C.W., and M.P.C. designed research; D.C., G.G., D.T., R.L., S.H., O.M.H.S.-A., S.F., G.M., D.G., A.L., C.F., C.P., S.M., D.F., R.G., and G.P. performed research; R.L. contributed new reagents/analytic tools; G.P., R.C.W., and P.M.C. analyzed data; and D.C., G.G., R.L., S.H., O.M.H.S.-A., S.F., G.M., A.L., C.P., S.M., D.F., R.G., G.P., R.C.W., and M.P.C. wrote the paper.

The authors declare no conflict of interest.

*This Direct Submission article had a prearranged editor.

Freely available online through the PNAS open access option.

[1]To whom correspondence may be addressed. E-mail: mariapaola.costi@unimore.it or rebecca.wade@h-its.org or glauco.ponterini@unimore.it.

See Author Summary on page 13889.

This article contains supporting information online at www.pnas.org/lookup/suppl/doi:10.1073/pnas.1104829108/-/DCSupplemental.

analysis, and isothermal titration calorimetry. This mechanism differs from those of protein–protein interface inhibitors reported to date (5), because it involves stabilization of an inactive form of the catalytic protein. Unlike the existing drugs targeting hTS, 5-FU and pemetrexed (34), these peptides inhibit intracellular hTS as well as cell growth without leading to hTS overexpression when administered to ovarian cancer cells. These peptides are thus promising candidates for the development of more effective anticancer therapies with reduced potential for drug resistance development.

Results and Discussion

Peptide Design and Inhibition Kinetics. LcC20 is a 20-mer peptide with a sequence that corresponds to a β-hairpin structure at the dimer interface of *Lactobacillus casei* TS (LcTS). This peptide destabilizes the protein's dimeric assembly through an unknown mechanism and induces aggregation (11). We tested hC20 (residues 198–217) (Fig. 1*A*), the corresponding peptide from hTS, against hTS and measured an IC_{50} of 30 ± 6 μM. To obtain smaller peptides better suited to the derivation of therapeutic agents, hC20 was fragmented into seven 8-mers in steps of two amino-acid residues (Fig. 1*B*). An additional peptide, C8, which corresponds to residues 247–254 of an adjacent β-strand, was used to probe a different interface region and does not overlap in sequence with any of the hC20 interface peptides (35) (Fig. 1*A* and *SI Appendix*).

Kinetic experiments showed that none of the octapeptides inhibited *Escherichia coli* TS (EcTS) at concentrations between 0.1 and 2 mM (the concentrations were dependent on peptide solubility). The hTS enzyme, however, was inhibited by peptides LN, LR, CG, YS, and C8, with inhibition percentages (I% at 100 μM peptide concentration) between 20 and 85% (Fig. 1*B*). In contrast, peptides VQ, QE, and SY were inactive at 100 μM. LR, CG, and C8 were investigated in more detail by running kinetic competition experiments with dUMP and mTHF. Dixon plots featured straight lines that intersected in the second quadrant. For experiments in which dUMP was the competitive substrate, values of K_i obtained from abscissa intersections in the mixed-type inhibition model (36) were 26 ± 2, 81 ± 3, and 41 ± 3 μM for LR, CG, and C8, respectively (see Fig. 1*C* and *SI Appendix*). After comparing these results with the sequences in Fig. 1*B*, we concluded that the residues close to the N and C termini of hC20, rather than the residues in the hairpin turn, were important for the inhibitory activity.

Secondary structure predictions and molecular dynamics (MD) simulations indicated that all of the octapeptides are flexible and mostly unstructured in aqueous solution (*Computational Studies* in *SI Appendix*). This behavior was confirmed by their circular dichroism (CD) spectra in water. In the presence of an increasing percentage of the structure inducer, 2,2,2-trifluoroethanol (TFE), the CD spectra of the peptides that inhibited hTS (LN, LR, CG, and C8) showed a transition from unordered structures to features of secondary structure (α-helices and, for

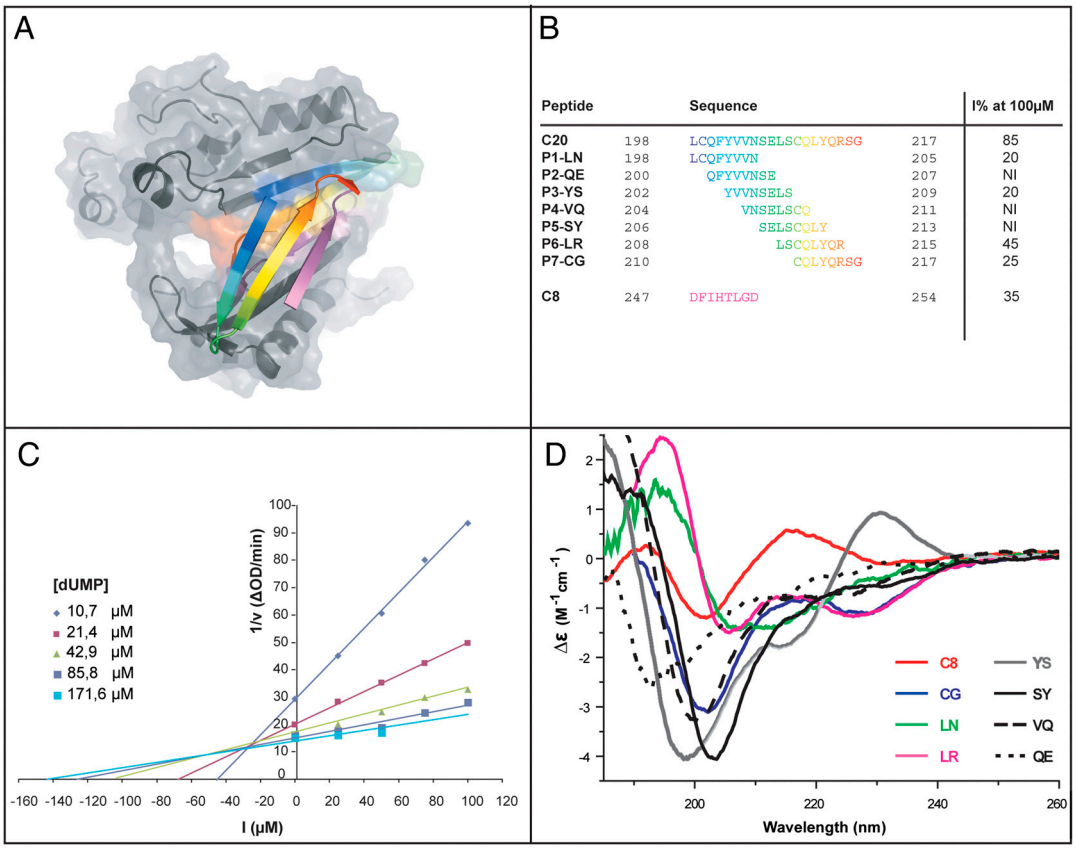

Fig. 1. Peptide design and characterization. (*A*) Interface location of peptide sequences in the crystal structure of hTS. For clarity, only subunit A of hTS (shown as a gray surface with ribbons) plus the regions corresponding to the hC20 and C8 peptides of subunit B (shown as rainbow and violet colored highlighted ribbons, respectively) are shown. (*B*) Seven octameric peptides (referred to by their first and last residues) were designed to cover the complete sequence of hC20 with an overlap of six residues. The coloring scheme follows Fig. 1*A* and measured percentage inhibition values are given. (*C*) Dixon plot, obtained from kinetic inhibition studies, showing mixed-type inhibition of hTS in the presence of different concentrations of the LR peptide (I, x-axis) and different concentrations of dUMP substrate for the differently coloured lines. (*D*) The CD spectra of the inhibitory peptides (colored lines) show secondary structure, whereas the spectra of the inactive peptides (black lines) do not. The spectrum for the YS peptide is shown in gray because, although it shows some inhibitory activity, its spectrum revealed little secondary structure.

C8, a polyproline type I helix), whereas the CD spectra of the inactive peptides (QE, SY, VQ) remained almost unchanged (Fig. 1*D* and *SI Appendix*). The propensity of the eight octapeptides to assume secondary structures correlated with their inhibitory activities. Previous studies have shown entropy-mediated gains in affinity by constraining the conformational freedom of ligands (37–42). In the present study, spontaneous prestructuring of the peptide might reduce the entropic penalty associated with formation of a peptide/hTS complex.

The LR Peptide Binds at a Previously Unknown Binding Site at the Dimer Interface of hTS in the Inactive Conformation. Crystallization trials for hTS complexed with the active peptides, LN, LR, CG, and C8, resulted only in crystals suitable for X-ray crystallography experiments for the hTS-LR complex. The structure was solved (Fig. 2*A* and Table S3 and *Methods* in *SI Appendix*) and revealed a previously undescribed peptide binding site. The electron density corresponding to the LR peptide spans a cleft located at the interface between the two subunits, which is defined by loops 188–194 of subunit A, the β-strands 175–181 of subunit B, and loops 142–157 of both subunits (hTS 1YPV numbering). The cleft includes Cys180 and is close to the catalytic Cys195, which points toward the dimer interface (14, 15). The crystal structures determined of hTS-LR and of uncomplexed hTS were compared by least-squares superimposition (PDB ID codes 3N5E and 3N5G, respectively). The average rmsd of the Cα-atoms between the LR-complexed structure and the uncomplexed di-inactive structure was about 0.2 Å. As expected, the largest deviations for the backbone atoms (1.5–2.0 Å) occurred in the loop regions close to the LR binding site (e.g., the Cα atoms of Glu145 and Asp148). Crystallographic refinement showed that the hTS-LR crystals belonged to the $P3_1$ space group rather than the $P3_121$ space group found in other hTS crystal structures (13). Indeed, the binding of one LR molecule per hTS dimer destroyed the crystallographic twofold symmetry. The LR peptide was buried in the binding cleft and covered by the side chains of Met190, Ala191, and Leu192 of subunit A, which were involved in hydrophobic interactions with Phe142 and Val158 of subunit B (Fig. 2*B*). Thus, the formation of the hTS-LR complex likely requires breathing movements in the region involved in the binding that controls the opening and closing of the protein dimer. Superposition of the present structure with a structure of hTS in an active conformation (1HVY) shows that the crevice at the dimer interface where LR is bound does exist in the active conformation but is narrower; in the hTS-LR structure, the loop 142–159 is more open by about 5 Å and the crevice is wider (see Table 1 and *SI Appendix*). Furthermore, MD simulations started from an inactive-uncomplexed form of hTS, show that the interfacial peptide binding site is widened when peptide is bound: The distance between the two peptide-flanking Trp180 residues increased by approximately 3 Å in the presence of LR (see *Computational Studies* in *SI Appendix*).

A Previously Undescribed Mechanism of hTS Inhibition. The structural information above suggests that the inhibitory effects of the active octapeptides might be a result of their ability to stabilize the di-inactive form of the enzyme, thereby increasing its equilibrium concentration (14, 15). The possibility that they may act as dissociative inhibitors can be ruled out because fluorescence resonance energy transfer (FRET) experiments, performed as described in ref. 16, show that they do not promote dissociation of the hTS dimer into monomers (*SI Appendix*).

To test the inhibition hypothesis given above, the binding of LR to hTS was characterized by isothermal titration calorimetry (ITC) (see Fig. 3*A*). Several binding models were tested (*Isothermal Titration Calorimetry* in *SI Appendix*) and an excellent fit (Fig. 3*A*, *Bottom*) was achieved with a consecutive, nonidentical, two-binding-site thermodynamic model in which only one form of the protein, with an abundance of approximately 1/3 interacted with the peptide. The hTS form that was able to bind the peptide did not interconvert with other protein forms on the time scale of the experiments (minutes). The best fit values of the thermodynamic parameters show that while both the enthalpic and the entropic contributions are large for the first binding site (b1), only the entropic contribution is large for the second one (b2).

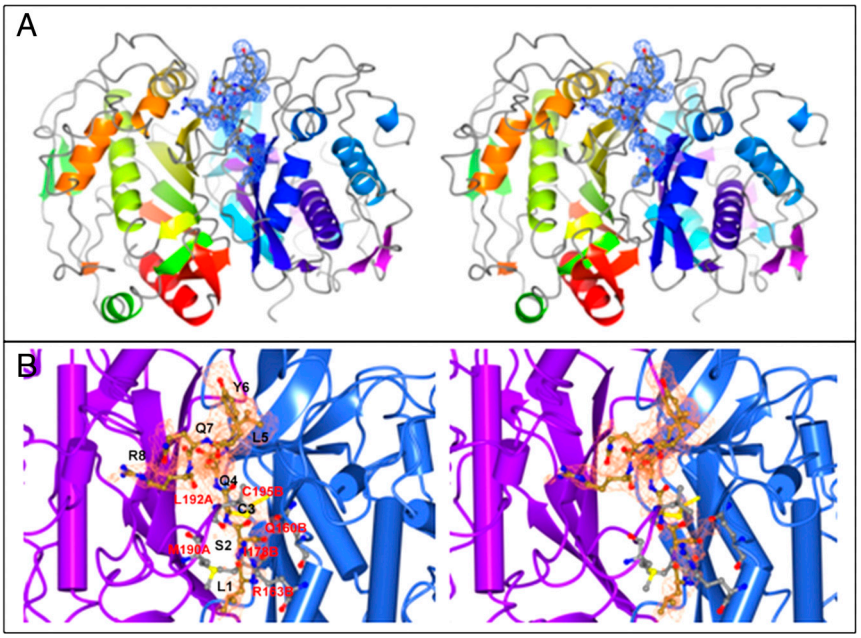

Fig. 2. X-ray crystal structure of the ht-hTS-LR complex. (*A*) Stereo view of the whole molecule with the LR peptide (ball and stick representation: carbon atoms are coral, nitrogen is blue, oxygen is red and sulfur is yellow) bound to the hTS dimer interface. LR is surrounded by the omit map (blue) contoured at 2.5 σ. Subunits A and B are represented as ribbons, with color ramping from green to red and from violet to blue, respectively. (*B*) Stereo view reporting a close up of the omit map (coral wire) contoured at 2.5 σ and superimposed to a ball and stick model of the LR peptide (ball and stick representation as above). The two independent subunits of hTS are represented as ribbons and cylinders (subunit A: magenta; subunit B: light blue).

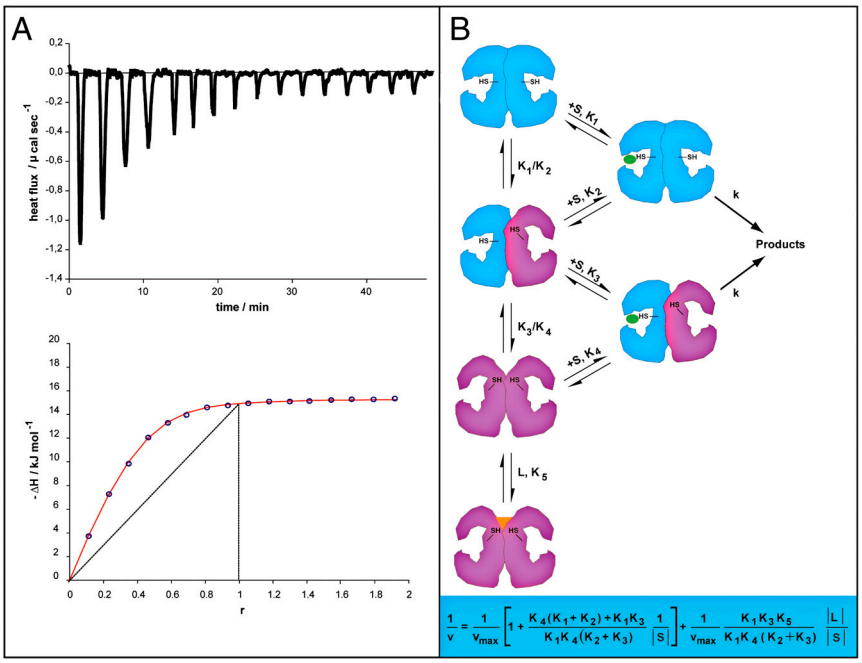

Fig. 3. hTS-LR peptide binding thermodynamics and proposed mechanism of hTS inhibition. (*A*) Top: Raw data from ITC experiments at 25 °C showing the heat flux recorded for each titration. Bottom: ΔH-vs-r plot where ΔH is the cumulative enthalpy (sum of the peak areas in the top panel) expressed per mole of protein and **r** is the concentration ratio of total titrated ligand to total protein. The red line represents the best fit of the experimental data (circles) using a thermodynamic model with two species of the protein with a constant population ratio, one of which presents two consecutive binding sites. A fixed stoichiometry of one ligand per binding site was assumed. Errors are within 10% of the reported values. The thermodynamic data for the first and second binding sites, respectively, are: $K_{b1} = 6.6 \times 10^6$ M^{-1} ($K_{d1} = 151$ nM), $\Delta H_1 = -12.3$ kJ/mol, $T\Delta S_1 = 26.6$ kJ/mol, $\Delta G° = -38.9$ kJ/mol1, and $K_{b2} = 7.8 \times 10^5$ M^{-1} ($K_{d2} = 1.3$ µM), $\Delta H_2 = -3.1$ kJ/mol, $T\Delta S_2 = 30.5$ kJ/mol, $\Delta G° = -33.6$ kJ/mol2. (*B*) Schematic diagram of the proposed mechanism of hTS inhibition in which the dimeric protein is represented by active (light blue) and inactive (magenta) subunits that interact with the substrate ($S \equiv$ dUMP, green) and the inhibitor ($L \equiv$ peptide, orange). The fractions of free monomers, of di-active protein with both active sites occupied by a substrate, and of di-inactive protein with two L molecules bound are assumed to be negligible.

Because of the weaker and entropic nature of the second binding, crystals of the hTS-LR$_2$ complex may be difficult to obtain (43).

We propose that the octapeptides bind only the di-inactive form of the protein on the basis of the following evidence: They do not inhibit EcTS, an enzyme that has never been observed in an inactive form; crystallographic results show that hTS is in the di-inactive form when bound to LR; the one-third fraction of the protein form able to bind the peptide according to the ITC results in 20 mM phosphate ion solution is consistent with the *ca.* 0.36 di-inactive protein fraction corresponding to a 60% abundance of the inactive form of hTS monomers, estimated from fluorescence data in this buffer (14, 44), under the assumption that in the dimeric protein, the probability that a monomer be found in a particular conformation, whether active or inactive, is independent of the conformation of the other monomer. Furthermore, we did not observe a calorimetric signal when LR was titrated into an hTS sample that was presaturated with dUMP, consistent with the fact that dUMP is expected to convert all of the protein into the active form (44) (*SI Appendix*). Upon computational docking of the LR peptide to the hTS dimer, the LR peptide was found predominantly at the dimer interface. While a docking pose was found close to the crystallographically observed site in the di-inactive form, docking poses were also found on the opposite side of the dimer interface (*SI Appendix*). The docking results thus support the hypothesis that two peptides could bind to different sites at the dimer interface of the inactive conformation of hTS.

The results from X-ray crystallography, computational modeling, and calorimetry provide evidence for a previously undescribed allosteric inhibitory mechanism for hTS. We propose the kinetic scheme shown in Fig. 3*B* for the interaction of LR with hTS. This is a special case of a more general mechanistic scheme provided in *Analysis of the kinetics of hTS inhibition by LR* in *SI Appendix*. In the general scheme, the enzyme is assumed to take several different forms, some of which are catalytically inactive and can bind ligands that contribute to their stabilization. According to the kinetic scheme in Fig. 3*B*, the peptide only binds the di-inactive form of the enzyme and stabilizes it. Analysis of this mechanism yields the Dixon-plot equation in Fig. 3*B* (see *SI Appendix* for a derivation). In this scheme, S is the concentration of dUMP (the variable-concentration substrate), and the protein is assumed to be presaturated with the mTHF substrate. The equation describes a family of straight lines that cross in the second quadrant and is therefore fully consistent with the inhibition pattern exhibited by LR (Fig. 1*C*), CG, and C8 (*SI Appendix*). From the intersection of the plot for LR, ($[L]_i = -[K_4(K_1 + K_2) + K_1K_3]/K_1K_3K_5$ and $v_i^{-1} = v_{\max}{}^{-1}$), and the kinetic data analysis outlined in *SI Appendix*, we obtained $v_{\max} = 0.22 \pm 0.04$ µM/s, which corresponds to the catalytic constant, $k = 0.8 \pm 0.15$ s^{-1}. Assuming K_1, K_2, K_3, and K_4 in Fig. 3*B* have the same value, K, we estimated this value to be approximately $K = 1 \times 10^5$ M^{-1} ($K^{-1} \sim 10$ µM). These parameters are comparable with the catalytic rate constant and K_M values obtained in the absence of inhibitor (i.e., $k = 0.9 \pm 0.2$ s^{-1} and $K_M = 11 \pm 1$ µM). Furthermore (see *SI Appendix*), we estimate a value of $K_5 = 1.1 \times 10^5$ M^{-1} for LR peptide binding (dissociation constant, $K_5{}^{-1} \sim 10$ µM). This value for K_5 is more than one order of magnitude lower than the first binding constant, K_{b1}, obtained from ITC ($K_{b1} = 6.6 \times 10^6$ M^{-1}, $K_{d1} = 151$ nM). The discussion of the consistency of this inhibition mechanism with the ITC model is complex. The mechanism requires a fast active-inactive interconversion for inhibition to occur. On the other hand, the ITC model requires that the active-inactive interconversion be slow compared with the ITC time scale. An important difference between the kinetic and calorimetric experiments is that, to avoid the catalyzed reaction, calorimetric titrations with

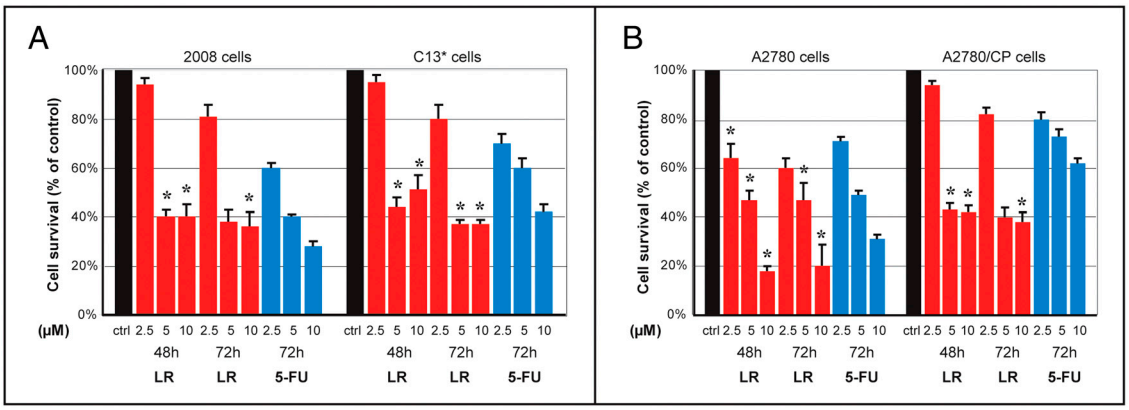

Fig. 4. Inhibition of cell growth by the LR peptide and 5FU for cDDP-sensitive and -resistant cells. (*A*) 2008 and C13* cells; (*B*) A2780 and A2780/CP cells. The concentration of LR (red) or 5-FU (blue) is given on the x-axis in μM. The LR Peptide was transfected into cells via a peptide delivery system. Cell survival percentages are the mean ± S.E.M. of at least three separate experiments performed in duplicate. Results were analyzed with Student *t* tests. $*P < 0.05$ compared with control cells.

dUMP were carried out in the absence of mTHF. Therefore, consistency of the proposed kinetic and calorimetric models relies on the assumption that mTHF accelerates the active-inactive interconversion, making it quicker than the time scale of the kinetic experiments.

Peptides Inhibit hTS in Ovarian Cancer Cells Without Resulting in hTS Protein Overexpression. The peptides that were active in the enzymatic kinetic assays (LN, YS, LR, CG, and C8) were tested against hTS in cellular extracts from untreated cells. Although LN and CG displayed little or no inhibition of enzyme activity in the cDDP-sensitive and -resistant cell extracts (inhibition range 10–35%), YS, C8, and LR showed higher inhibitory activity against the enzyme in both cell lines (inhibition range 50–70%) comparable with the I% against the recombinant protein that was (I% at 100 μM peptide concentration) between 20 and 85%. The peptides alone did not enter the cells. To test their effects on cell growth, we employed a delivery system that we checked did not alter cell growth itself. Administration of 5–10 μM of YS, C8, or LR (the peptides most active against hTS in cell extracts) significantly ($*P < 0.05$, $n = 5$) inhibited the growth of all cell lines by about 50% (*SI Appendix*). The YS and LR peptides appeared particularly active against A2780 cells.

Of these active peptides, we focused on LR because of the availability of crystallographic information on its complex with hTS. At 5 and 10 μM, LR inhibited the growth of both sensitive and resistant cell lines by approximately 50% after both 48- and 72-h exposures (Fig. 4). A higher cell death was caused by 10 μM LR for the A2780 line. With the latter cell line and its resistant counterpart, LR turned out to be more effective than 5-FU at the same concentration (Fig. 4*B*).

Information on the mode of action of these peptides in cells was provided by measurement of the inhibition of cellular hTS and of protein and mRNA transcript levels. Upon incubation with ovarian cancer cells, LR inhibited the intracellular enzyme activity quite markedly, though less efficiently than 5-FU; the effect was more pronounced in the sensitive cells (Fig. 5*A*).

To verify whether an impairment of intracellular enzyme activity and of cell growth was reflected by the levels of enzyme expression (Fig. 5*B*) and RNA (Fig. 5*C*), these were determined under the same experimental conditions. The total hTS protein level was increased by 5-FU exposure in both cell lines, which has been suggested to be due to the formation of the inactive ternary complex hTS-FdUMP-mTHF (45). In contrast, 20 μM LR decreased the total hTS protein level by about 25% in sensitive cells and did not affect the protein level in the resistant cells (Fig. 5*B*). The level of hTS mRNA was about the same in the presence of both LR and 5-FU in resistant cells while it was higher in sensitive cells (Fig. 5*C*). The overexpression of hTS mRNA in sensitive cells likely resulted from a transcriptional induction following the downstream inhibition of TS protein. LR also decreased the level of dihydrofolate reductase (DHFR), another important enzyme in the folate pathway (46), although not as markedly as 5-FU (Fig. 5*B*). Interestingly, LR did not inhibit the hDHFR recombinant protein. The LR-induced decrease in hDHFR levels in the cells might result from a decrease of the dihydrofolate levels due to hTS inhibition.

Conclusions and Perspectives. We have identified several octapeptides that inhibit hTS. Of these, LR binds at a previously unidentified binding site located at the interface between the two monomers of the hTS homodimer and inhibits hTS by a previously undescribed mechanism of action. Rather than acting as a dissociative inhibitor, LR stabilizes the di-inactive form of the protein. The peptides that inhibit hTS have an inducible secondary structure and inhibit the growth of both cisplatin-sensitive and cisplatin-resistant ovarian cancer cell lines. In contrast to classical TS inhibitors (e.g., 5-FdUMP and pemetrexed), the peptides inhibit intracellular TS without inducing its overexpression.

The connection between the stabilization of the inactive form of hTS by LR and the cellular effects remains to be fully explored. Further steps will require optimization of the compounds by synthesis of peptidomimetics and detailed analysis of their cellular mechanism of action. To our knowledge, this is a unique demonstration of a mechanism in which a multifunctional homodimeric protein is inhibited through binding of a ligand to the dimer interface of the di-inactive conformation of the enzyme, resulting in stabilization of this form. We believe that the concepts revealed here can be exploited to provide new avenues for the development of drugs for combating severe diseases such as ovarian cancer.

Methods

Chemicals and Peptides. hC20 and LR peptides were synthesised by an automatic solid phase peptide synthesiser (Syro XP II, Multisyntech) using Fmoc/tBu chemistry (47). The peptides were cleaved from the resin using reagent B (48). Crude peptides were purified by preparative reverse-phase HPLC, and the purity grade was checked by analytical HPLC analyses and mass spectrometry (see *Methods* in *SI Appendix*). All other peptides employed in this study were purchased from GeneCust (www.genecust.com). The level of purity of peptides was >95%. The peptides were further purified before use to remove trifluoroacetic acid residues. dUMP and mTHF were purchased from Sigma-Aldrich.

Protein Cloning and Purification. hTS was purified from the *E. coli* BL21 strain DH5α transformed with pQE80L, which contained the complete coding sequence for the hTS tagged with a histidine tail (ht-hTS). Purification involved sequential chromatography on an Ni Sepharose 6 Fast Flow resin

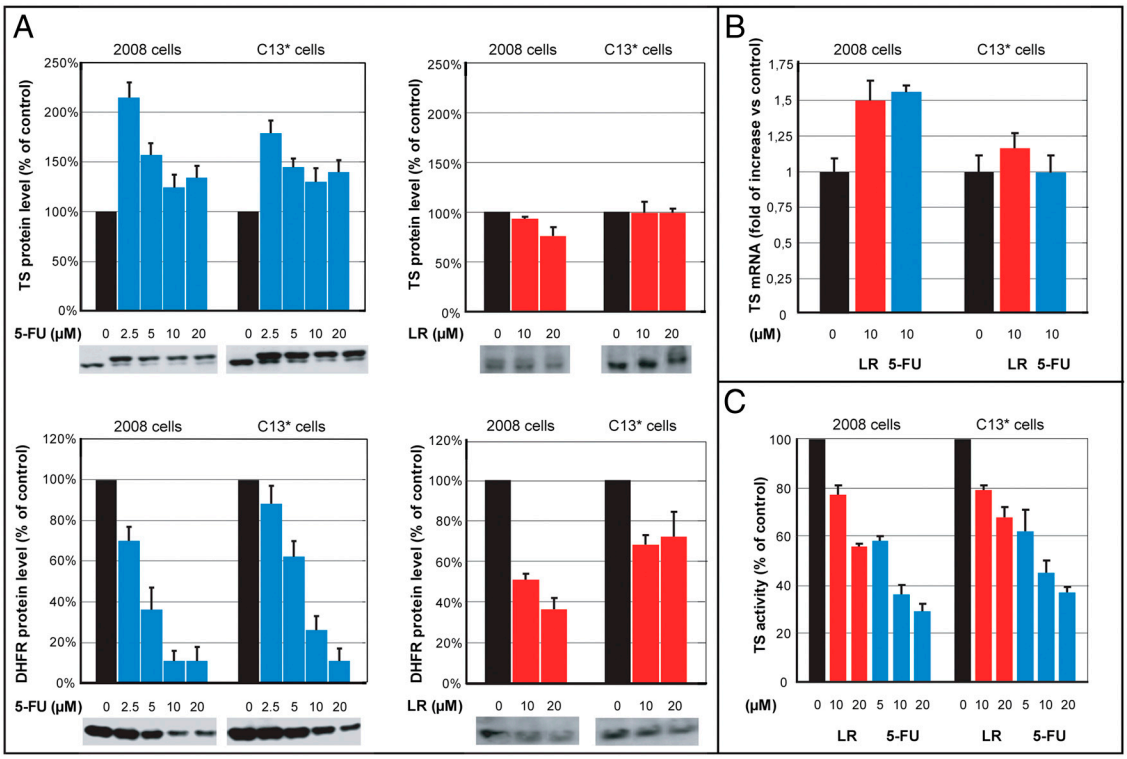

Fig. 5. Effects of LR and 5-FU on hTS and DHFR protein levels, hTS mRNA levels and hTS activity in two ovarian cancer cell lines. (*A*) Western immunoblot analysis of hTS (above) and DHFR (below) protein levels from 2008 and C13* cells treated for 72 h with the indicated concentrations of 5-FU (blue) and LR peptide (red). The latter was administered via a peptide delivery system. The 35-kDa hTS monomer, with or without its ternary complex, and the 21-kDa hDHFR monomer are reported below the bar graphs of their respective densitometric analyses. Western blot analyses were performed on cytosolic extracts from cells in the exponential phase of growth using anti-hTS and DHFR monoclonal antibodies. Each experiment was carried out three times, and a representative result is shown. An antihuman ß-tubulin mouse antibody was used to verify equal protein loading in the gel. (*B*) RT-PCR analysis of hTS mRNA levels. hTS expression in 2008 and C13* cells extracts was determined after treatment with the LR peptide or 5-FU for 72 h. The amount of hTS mRNA was normalized by the mRNA of glyceraldehyde-3-phosphate dehydrogenase. The results shown are the means ± S.E.M. of four separate experiments performed in duplicate. (*C*) Inhibition of intracellular TS activity.

column and a HiTrap desalting column, which were both purchased from GE Healthcare (www.gehealthcare.com). *Ec*TS was purified through ammonium sulphate precipitation and sequential chromatography using DEAE Sephacel and Phenylsepharose CL-4B resin. The protein concentrations were determined spectrophotometrically from absorbance at 280 nm ($\epsilon_{280} = 89{,}000\ M^{-1}\ cm^{-1}$).

Enzyme Kinetics. Various concentrations of peptides were incubated with hTS and EcTS in phosphate buffer (pH 6.9) at 25 °C. Aliquots of the enzyme were assayed for activity under standard conditions: An aliquot of TS (0.5–1 μg) was added to 1 mL of assay buffer consisting of 50 mM TES (pH 7.4) containing 25 mM $MgCl_2$, 6.5 mM HCHO, 1 mM EDTA, 75 mM β-mercaptoethanol (β-ME), 0.120 mM dUMP, and 0.15 mM mTHF. Following addition of the enzyme, the absorbance was monitored at 340 nm for 4 min.

Circular Dichroism. CD spectra were recorded on a JASCO-J-810 spectropolarimeter in quartz cells with path lengths of either 0.1 or 1 cm using the following parameters: 4 s response; 50 nm/min scan speed; 0.1 nm data pitch; 2 accumulations; 1 nm bandwidth. Spectra were corrected by subtracting the cell and solvent contributions and were smoothed using a standard noise reduction routine provided with the instrument. Stock peptide solutions approximately 500 μM were prepared in pure Milli-Q water or pure TFE. The peptide concentrations were checked spectrophotometrically using the maximum molar extinction coefficient values for Tyr ($\epsilon = 1440\ M^{-1}\ cm^{-1}$ at 274 nm) and Phe ($\epsilon = 220\ M^{-1}\ cm^{-1}$ at 257 nm). All spectra were measured within half an hour from solution preparation.

Crystallography. The histidine-tagged construct (ht-hTS) consisted of the complete sequence of hTS (SwissProt entry: P04818) with the MRGSHHHHHHGS sequence added at the N terminus, which resulted in a total of 325 amino-acid residues and a molecular weight of 37,114 Da. ht-hTS has a dimeric quaternary structure, which was indicated by gel-filtration chromatography and confirmed by crystal structure determination. Crystals of ht-hTS were obtained using a sitting drop setup using as precipitant a 20–25% saturated $(NH_4)_2SO_4$ buffered at pH 8.3 (see *SI Appendix* for details). Crystals of the ht-hTS complex with the LR peptide (LSCQLYQR; ht-hTS-LR) were grown in the same setup and precipitant conditions from a ht-hTS solution incubated for 2 h at 4 °C with a 1 mM solution of the LR peptide in water (see *SI Appendix* for details). The ht-hTS and ht-hTSLR crystals displayed the same habit and belong to the trigonal system. Crystallographic data were collected at 100 K on frozen crystals upon cryoprotection. The data collection was performed at ESRF (Grenoble) on beamlines ID 14-1 and ID 23-1.The crystals were stable in the beam over the data collection time (approximately 25 min), and one crystal was used for each dataset. See *SI Appendix* and Table S3 in *SI Appendix* for details and final data collection statistics. The two structures were solved using the molecular replacement technique (49) using as model one subunit of human TS (50) (PDB ID code 1YPV) for ht-hTS and using ht-hTS as model for the ht-hTS-LR complex. The refinement was carried out by using REFMAC5 (51). Between the refinement cycles, the models were subjected to manual rebuilding using Xtal (52) and Coot (53). The program Coot has been used to model the LR peptide. The structure of ht-hTS belongs to the trigonal space group $P3_121$ where the twofold axis of the ht-hTS dimer coincides with the crystallographic twofold axis. The formation of a 1:1 complex between the ht-hTS dimer and the LR peptide should remove the twofold symmetry present in the enzyme. In order to ascertain if the symmetry of the ht-hTS-LR crystal was effectively lowered to $P3_1$, we processed and refined the data in both $P3_121$ and $P3_1$ space groups. The final R_{cryst} and R_{free} factors converged to lower values for the structure in $P3_1$ indicating that ht-hTS-LR belongs to this space group. Additional details about structure solution and refinement are reported in *SI Appendix* and the refinement statistics are shown in Table S3 in *SI Appendix*.

Fluorescence. Fluorescence resonance energy transfer experiments were carried out on hTS difunctionalized with an excitation-energy donor, fluorescein (F), and an acceptor, tetramethyl rhodamine (T). The protocol employed to conjugate the two probes to the dimeric protein, the structural aspects

(the two probes bind at C43 and C43′) and the quantitative analysis of the steady-state fluorescence data are described in detail in ref. 16. Solutions of the diconjugated protein in phosphate buffer, pH 7.5, were checked at the UV-visible spectrophotometer (Varian Cary 100) to contain comparable concentrations (typically *ca.* 350 nM) of each of the two probes, F and T, and of protein dimers. Emission spectra at $\lambda_{exc} = 450$ nm of these solutions were recorded at different peptide concentrations on a Jobin-Yvon Fluoromax2 spectrofluorometer and were corrected for the instrumental spectral sensitivity.

Isothermal Titration Calorimetry. The calorimetric experiments were performed on a MicroCal® (www.microcal.com) VP-ITC MicroCalorimeter. The enzyme solution was thawed on the day of experiment and its concentration was checked spectrophotometrically at 280 nm. It was then degassed for 8 min under magnetic stirring, filtered with a 0.45 μm filter, and loaded inside the sample cell of the instrument. 8-mer peptides were dissolved in experimental buffer at the desired concentration the day before the experiment and the solutions were left under magnetic stirring at 4 °C. The solutions were filtered with a 0.45 μm filter and loaded in the injection syringe.

Experiments were initiated by filling the reference cell with 1.5 mL of double distilled Milli-Q water and the sample cell with 1.5 mL of hTS solution (10, 20, and 40 μM) in phosphate buffer (20 mM NaH_2PO_4, 30 mM NaCl, pH 7.5). Titration of LR (1 mM) was carried out at 298 K via a rotating stirrer-syringe. The injection volume was 10 μL and an equilibrium time of 4 min was allowed between each injection. The total number of injections was 25. Blank titrations were performed by injecting the ligand into the buffer devoid of protein to correct for the heat of mixing and ligand dilution. This contribution to the observed heat of reaction was subtracted from the corresponding total heat. The heat arising from enzyme dilution due to titrant injection was negligible in all cases. See *SI Appendix* for data analysis. For the titration of LR against the hTS-dUMP complex, 0.052 mM solution of hTS in phosphate buffer was incubated for 1 h with dUMP at saturating concentrations (3,000 μM) prior to the titration.

Computational Methods. The helical content of the peptides was predicted with the AGADIR algorithm (54). MD simulations were carried out of peptides and hTS-peptide complexes in water with the AMBER simulation package (55) using the AMBER ff03 forcefield (56). Peptides were docked to hTS with the program GOLD (57) using the ChemScore scoring function. For details, see *Methods* in *SI Appendix*.

Experiments with Cells. The 2008 cell line was established from a patient with serous cystadenocarcinoma of the ovary. The cDDP-resistant C13* subline, approximately 15 times more resistant to cDDP than a normal cell line, was derived from the parent 2008 cell line as previously reported (58). The human ovarian carcinoma A2780/CP cells were 12-fold resistant to cDDP and derived from the parent A2780 cell line. Peptides were delivered into cells via the SAINT-PhD peptide delivery system (Synvolux Therapeutics B. V.). Cells that were used for the enzyme assay were treated according to procedures published by van Triest et al. (59). The crystal violet dye assay was performed on a cell monolayer (60). Western blot analysis on TS and DHFR proteins was conducted as previously described (61). Reverse transcription was performed with 2 μg of total RNA, and RT-PCR was performed with 10 ng of cDNA using the Power SYBR® Green PCR Master Mix (Applied Biosystems). This was followed by a dissociation curve analysis and agarose gel electrophoresis to confirm the amplification (62). Statistical significance was estimated by a two-tailed Student's *t* test using Microsoft Excel. A P value <0.05 was considered significant.

ACKNOWLEDGMENTS. We thank Yap Boum and Hannu Myllykallio for synthetic gene constructs for expressing histidine-tagged human thymidylate synthase in *E. coli* (GenBank: EU520475.1). This work was financially supported by the European Union (LIGHTS project: LSH-2005-2.2.0-8), the Italian Association for Cancer Research (IG 10474 to P.M.C.), the Klaus Tschira Foundation (R.C.W., S.H., O.M.H.S-A), and O.M.H.S-A. also received funding from the Alexander von Humboldt Foundation, the Finnish Cultural Foundation, the Academy of Finland, and the University of Kuopio.

1. Nooren IM, Thornton JM (2003) Diversity of protein–protein interactions. *EMBO J* 22:3486–3492.
2. Caffrey DR, Somaroo S, Hughes JD, Mintseris J, Huang ES (2004) Are protein–protein interfaces more conserved in sequence than the rest of the protein surface? *Protein Sci* 13:190–202.
3. Chène P (2007) *Chemical Biology: From Small Molecules to System Biology and Drug Design*, eds SL Kapoor, TM Schreiber, and G Wess (Wiley-VCH, Weinheim), ch 15, 3, pp 979–1002.
4. Jones S, Thornton JM (1995) Protein–protein interactions: A review of protein dimer structures. *Prog Biophys Mol Biol* 63:31–65.
5. Cardinale D, et al. (2010) Homodimeric enzymes as drug targets. *Curr Med Chem* 17:826–846.
6. de Vega MJ, Martin-Martinez M, Gonzalez-Muniz R (2007) Modulation of protein–protein interactions by stabilizing/mimicking protein secondary structure elements. *Curr Top Med Chem* 7:33–62.
7. Fletcher S, Hamilton AD (2006) Targeting protein–protein interactions by rational design: Mimicry of protein surfaces. *J R Soc Interface* 3:215–233.
8. Loregian A, Palu G (2005) Disruption of protein–protein interactions: Towards new targets for chemotherapy. *J Cell Physiol* 204:750–762.
9. Yin HH (2007) *Chemical Biology: From Small Molecules to System Biology and Drug Design*, eds SL Kapoor, TM Schreiber, and G Wess (Wiley-VCH, Weinheim), ch 43, 1, pp 250–270.
10. Sillerud LO, Larson RS (2005) Design and structure of peptide and peptidomimetic antagonists of protein-protein interaction. *Curr Protein Pept Sci* 6:151–169.
11. Prasanna V, Bhattacharjya S, Balaram P (1998) Synthetic interface peptides as inactivators of multimeric enzymes: inhibitory and conformational properties of three fragments from Lactobacillus casei thymidylate synthase. *Biochemistry* 37:6883–6893.
12. Carreras CW, Santi DV (1995) The catalytic mechanism and structure of thymidylate synthase. *Annu Rev Biochem* 64:721–762.
13. Schiffer CA, Clifton IJ, Davisson VJ, Santi DV, Stroud RM (1995) Crystal structure of human thymidylate synthase: A structural mechanism for guiding substrates into the active site. *Biochemistry* 34:16279–16287.
14. Phan J, et al. (2001) Structure of human thymidylate synthase suggests advantages of chemotherapy with noncompetitive inhibitors. *J Biol Chem* 276:14170–14177.
15. Berger SH, Berger FG, Lebioda L (2004) Effects of ligand binding and conformational switching on intracellular stability of human thymidylate synthase. *Biochim Biophys Acta* 1696:15–22.
16. Genovese F, et al. (2010) Dimer-monomer equilibrium of human thymidylate synthase monitored by fluorescence resonance energy transfer. *Protein Sci* 19:1023–1030.
17. Danenberg PV, Malli H, Swenson S (1999) Thymidylate synthase inhibitors. *Semin Oncol* 26:621–631.
18. Chu E, Allegra CJ (1996) The role of thymidylate synthase as an RNA binding protein. *Bioessays* 18:191–198.
19. Chu E, et al. (1991) Autoregulation of human thymidylate synthase messenger RNA translation by thymidylate synthase. *Proc Natl Acad Sci USA* 88:8977–8981.
20. Chu E, et al. (1993) Identification of an RNA binding site for human thymidylate synthase. *Proc Natl Acad Sci USA* 90:517–521.
21. Liu J, et al. (2002) Thymidylate synthase as a translational regulator of cellular gene expression. *Biochim Biophys Acta* 1587:174–182.
22. Ju J, Pedersen-Lane J, Maley F, Chu E (1999) Regulation of p53 expression by thymidylate synthase. *Proc Natl Acad Sci USA* 96:3769–3774.
23. Ozasa H, et al. (2010) Significance of thymidylate synthase for resistance to pemetrexed in lung cancer. *Cancer Sci* 101:161–166.
24. Chu E, Callender MA, Farrell MP, Schmitz JC (2003) Thymidylate synthase inhibitors as anticancer agents: From bench to bedside. *Cancer Chemother Pharmacol* 52(Suppl 1):80–89.
25. Kitchens ME, Forsthoefel AM, Rafique Z, Spencer HT, Berger FG (1999) Ligand-mediated induction of thymidylate synthase occurs by enzyme stabilization. Implications for autoregulation of translation. *J Biol Chem* 274:12544–12547.
26. Ozols RF, et al. (2003) Specific keynote: Chemoprevention of ovarian cancer: the journey begins. *Gynecol Oncol* 88:S59–66 discussion S67-70.
27. Ozols RF, Markman M, Thigpen JT (2002) ICON3 and chemotherapy for ovarian cancer. *Lancet* 360:2086–2087.
28. Scanlon KJ, Kashani-Sabet M (1988) Elevated expression of thymidylate synthase cycle genes in cisplatin-resistant human ovarian carcinoma A2780 cells. *Proc Natl Acad Sci USA* 85:650–653.
29. Scanlon KJ, Wang WZ, Han H (1990) Cyclosporin A suppresses cisplatin-induced oncogene expression in human cancer cells. *Cancer Treat Rev* 17(Suppl A):27–35.
30. Chu G (1994) Cellular responses to cisplatin. The roles of DNA-binding proteins and DNA repair. *J Biol Chem* 269:787–790.
31. Sehouli J, et al. (2010) A phase-I trial of pemetrexed plus carboplatin in recurrent ovarian cancer. *Cancer Chemother Pharmacol* 66:861–868.
32. Vergote I, et al. (2009) A randomised, double-blind, phase II study of two doses of pemetrexed in the treatment of platinum-resistant, epithelial ovarian or primary peritoneal cancer. *Eur J Cancer* 45:1415–1423.
33. Lovelace LL, Gibson LM, Lebioda L (2007) Cooperative inhibition of human thymidylate synthase by mixtures of active site binding and allosteric inhibitors. *Biochemistry* 46:2823–2830.
34. Peters GJ, et al. (2000) Molecular downstream events and induction of thymidylate synthase in mutant and wild-type p53 colon cancer cell lines after treatment with 5-fluorouracil and the thymidylate synthase inhibitor raltitrexed. *Eur J Cancer* 36:916–924.
35. Voeller DM, Zajac-Kaye M, Fisher RJ, Allegra CJ (2002) The identification of thymidylate synthase peptide domains located in the interface region that bind thymidylate synthase mRNA. *Biochem Biophys Res Commun* 297:24–31.
36. Segel IH (1993) *Enzyme Kinetics: Behavior and Analysis of Rapid Equilibrium and Steady State Enzyme Systems* (John Wiley and Sons, New York), ch 4, pp 161–226.
37. Chang YP, Chu YH (2005) Using surface plasmon resonance to directly determine binding affinities of combinatorially selected cyclopeptides and their linear analogs to a streptavidin chip. *Anal Biochem* 340:74–79.
38. Dathe M, Nikolenko H, Klose J, Bienert M (2004) Cyclization increases the antimicrobial activity and selectivity of arginine- and tryptophan-containing hexapeptides. *Biochemistry* 43:9140–9150.

39. Dumez E, et al. (2002) Synthesis of macrocyclic, potential protease inhibitors using a generic scaffold. *J Org Chem* 67:4882–4892.
40. Kang JH, et al. (2004) Macrocyclic diacylglycerol-bis-lactones as conformationally constrained analogues of diacylglycerol-lactones. Interactions with protein kinase C. *J Med Chem* 47:4000–4007.
41. Khan AR, et al. (1998) Lowering the entropic barrier for binding conformationally flexible inhibitors to enzymes. *Biochemistry* 37:16839–16845.
42. Nam NH, Ye G, Sun G, Parang K (2004) Conformationally constrained peptide analogues of pTyr-Glu-Glu-Ile as inhibitors of the Src SH2 domain binding. *J Med Chem* 47:3131–3141.
43. Capaldi S, et al. (2007) A single amino acid mutation in zebrafish (Danio rerio) liver bile acid-binding protein can change the stoichiometry of ligand binding. *J Biol Chem* 282:31008–31018.
44. Gibson LM, Lovelace LL, Lebioda L (2008) The R163K mutant of human thymidylate synthase is stabilized in an active conformation: Structural asymmetry and reactivity of cysteine 195. *Biochemistry* 47:4636–4643.
45. Marverti G, et al. (2009) Collateral sensitivity to novel thymidylate synthase inhibitors correlates with folate cycle enzymes impairment in cisplatin-resistant human ovarian cancer cells. *Eur J Pharmacol* 615:17–26.
46. Gmeiner WH (2005) Novel chemical strategies for thymidylate synthase inhibition. *Curr Med Chem* 12:191–202.
47. Benoiton NL (2005) *Chemistry of Peptide Synthesis* (Taylor & Francis, USA), pp 125–154.
48. Solé NA, Barany G (1992) Optimization of solid-phase synthesis of [Ala8]-dynorphin A. *J Org Chem* 57:5399–5403.
49. Vagin A, Teplyakov A (1997) MOLREP: An automated program for molecular replacement. *J Appl Crystallogr* 30:1022–1025.
50. Lovelace LL, Minor W, Lebioda L (2005) Structure of human thymidylate synthase under low-salt conditions. *Acta Crystallogr D Biol Crystallogr* 61:622–627.
51. Murshudov GN, Vagin AA, Dodson EJ (1997) Refinement of macromolecular structures by the maximum-likelihood method. *Acta Crystallogr D Biol Crystallogr* 53:240–255.
52. McRee DE (1999) XtalView/Xfit-A versatile program for manipulating atomic coordinates and electron density. *J Struct Biol* 125:156–165.
53. Emsley P, Cowtan K (2004) Coot: Model-building tools for molecular graphics. *Acta Crystallogr D Biol Crystallogr* 60:2126–2132.
54. Munoz V, Serrano L (1994) Elucidating the folding problem of helical peptides using empirical parameters. *Nat Struct Biol* 1:399–409.
55. Case DA, et al. (2005) The Amber biomolecular simulation programs. *J Comput Chem* 26:1668–1688.
56. Duan Y, et al. (2003) A point-charge force field for molecular mechanics simulations of proteins based on condensed-phase quantum mechanical calculations. *J Comput Chem* 24:1999–2012.
57. Jones G, Willett P, Glen RC, Leach AR, Taylor R (1997) Development and validation of a genetic algorithm for flexible docking. *J Mol Biol* 267:727–748.
58. Andrews PA, Albright KD (1992) Mitochondrial defects in cis-diamminedichloroplatinum(II)-resistant human ovarian carcinoma cells. *Cancer Res* 52:1895–1901.
59. van Triest B, et al. (1999) Thymidylate synthase level as the main predictive parameter for sensitivity to 5-fluorouracil, but not for folate-based thymidylate synthase inhibitors, in 13 nonselected colon cancer cell lines. *Clin Cancer Res* 5:643–654.
60. Kueng W, Silber E, Eppenberger U (1989) Quantification of cells cultured on 96-well plates. *Anal Biochem* 182:16–19.
61. Longley DB, et al. (2001) Characterization of a thymidylate synthase (TS)-inducible cell line: A model system for studying sensitivity to TS- and non-TS-targeted chemotherapies. *Clin Cancer Res* 7:3533–3539.
62. Arocho A, Chen B, Ladanyi M, Pan Q (2006) Validation of the 2-DeltaDeltaCt calculation as an alternate method of data analysis for quantitative PCR of BCR-ABL P210 transcripts. *Diagn Mol Pathol* 15:56–61.